50th AIAA Aerospace Sciences Meeting including the New Horizons Forum and Aerospace Exposi
9 - 12 January 2012, Nashville, Tennessee

AIAA 2012-300

Simulations of a pitch-up and pitch-down maneuver of a span-wise flexible wing in a free stream flow

Dewei Qi[1], Guowei He[2] & Yingming Liu[3]

December 19, 2011

[1]Department of Paper Engineering,Chemical Engineering and Imaging, Western Michigan University, Kalamazoo MI 49008, USA
[2] LNM, Institute of Mechanics, Chinese Academy of Sciences, Beijing, 100080, China
[3]Yangtze Center of Mathematics, Sichuan University, Chengdu 610064, China

Abstract

A span-wise flexible wing undergoing a rapid pitch-up and pitch-down maneuver in a steady free stream is studied with a lattice Boltzmann flexible particle method (LBFPM) in a three-dimensional space at a chord based Reynolds number of 100. The pitching rates and flexibility are systematically varied, and their effects on the generated aerodynamic forces and power efficiency are explored. It is found that at a higher pitch rate average lift coefficient increases first, as flexural rigidity decreases, and arrives at a maximum, then falls down as the flexural rigidity continuously decreases, while at a lower pitch rate, no similar phenomena is observed. It seems that flexibility can be utilized to improve lift at a high reduced frequency. A small deformation at a level of 5% due to flexibility can largely improve lift force only during pitch-down time period. On the Contrary, flexibility has a negative impact on the lift during pitch-up time period. Most likely, deformation may passively and dynamically adjust the trailing edge position along the span direction, induce larger leading edge vortices (LEV) and tip edge vortices (TEV), and enhance trailing vortex shedding due to Kutta condition, thus improve lift.

Nomenclature

ΔT	the holding period
ψ	the pitch angle
ρ_f	the density of fluid
t_1	the start time of the pitch-up
t_2	the end of the pitch-up
t_3	the start of the pitch-down
t_4	the end of the pitch-down
κ	the maximum of pitch angle
ψ_0	the freuency

ρ_s

c	the chord length
C_d	the drag coefficient
C_l	the lift coefficient
EI	the flexural rigidity
GI	the torsional rigidity
Re	the Reynolds number
Re_s	the rotational Reynolds number
s	the span length
T	the wing thickness
U_0	the velocity of free stream

1 Introduction and background

Mechanisms of biologically inspired insets fight recently becomes an important research subject, in particular, for potential usage of micro-scale vehicles in defense surveillance and environmental monitoring. Although prevailing challenge in understanding aerodynamics of insets flight comes from complex interactions among deformable wing, its periodically plunging (translation) and pitching (rotation) kinematics, and surrounding fluid flows, much progresses on the effects of flexibility on thrust, lift and flight efficiency have been achieved experimentally and numerically.

A moth wing as a linearly elastic structure was modeled using finite element analysis and a slight increases in lift during downstroke was found by Smith [1]. Experiments were conducted to investigate the effect of flexibility in the chord [2] and span-wise [3] directions on the thrust, lift and power efficiency by Heathcote et al. [4]. They found that the thrust coefficient of the airfoil with intermediate stiffness was greatest at high plunge frequency while least stiff airfoil generates a larger thrust at low frequency. Similarly, at an intermediate level of span-wise flexibility, a 50% of improvement in thrust coefficient was reported. Effects of bending and torsion on thrust were studied experimentally by Frampton et al. [5]. They found that a wing with in phase bending and torsional motion generated the largest thrust whereas a wing with the torsion motion lagging the bending motion by 90^0 delivered the best efficiency. A computational aero-elasticity framework for analyzing flapping wing in three dimensional space was presented by Chimakurthi et al.[6]. Their computational results for the flexibility in span-wise direction of a plunging wing were in good agreement with the experimental results of Heathcote et al. [3]. They confirmed that flexibility benefits the thrust force [7, 8, 9, 6, 10, 11].

Toomey and Eldredge [12], Eldredge et al [13], Vanella et al [14], used a two dimensional model wing with two and three rigid beam segments connected by a torsion spring through a hinge to simulate the motion of a chord-wise flexible wing. Eldredge et al found that wing flexion generally reduces the power consumed by flapping compared to a rigid wing. Toomey and Eldredge found that the rate and timing of wing rotation primarily controls the generation of lift in rapid rotation; in contrast, the translational acceleration has little effect. Vanella et al.[14] identified that the wing flexibility can enhance aerodynamic performance and that the optimization is realized when the wing is excited by a non-linear resonance at 1/3 of the natural frequency.

Very recently, the two-segment beam model in a two-dimensional space has been extend to a multi-segment beam model in a three dimensional space by Qi et al[15, 16]. They demonstrated that as the number of the beam segment increases, the multi-segment beam model can approximate the nonlinear Euler-Bernoulli beam equation and that the model, incorporated with lattice Boltzmann (LB) method, is suitable for simulation of aerodynamics associated with a flexible wing. This method is called lattice Boltzmann flexible particle method (LBFPM).

Using the LBFPM a numerical simulation of sinusoidal plunge and pitch of a span-wise flexible and a chord-wise flexible wing in hover without free-stream were conducted, respectively[16, 17] It was found that span-wise and chord wise flexibility could significantly improve lift forces due to a mixture of four mechanisms: wake capture, rotational[18], leading edge vortices (LEV) [19], and downwash flow leading a smaller effective angle of attach.

However, due to the complex interactions between large deformation and fluid flows, the question "to what extend and how does the flexibility affect each mechanism" is still open and remains a great challenge. To distinguish and quantify the different contribution from each of the four mechanisms to lift and drag forces due to flexibility, the kinematics of wing flapping should be simplified. It is possible that a pitch motion may be isolated from periodic plunge motion. A canonical kinematics with a pitch-up and pitch-down without periodic motion was suggested and used experimentally and numerically for rigid wings by many authors [20, 21, 22, 23, 24, 25, 26, 27, 28, 29]. Such the simplicity allows us focus on the effects of pitch only without considering the influence of the periodic plunge motion. This scheme may effectively reduce the number of variables and the degree of the difficulty in exploring all of the possible mechanics of aerodynamics, in particular, for a flexible wing. Only after understanding the pitch effect and its relationship with flexibility whole physical picture of complexity of flapping flight will be more easily captured and understood.

Therefore, the canonical kinematics will be adopted to simulate a span-wise flexible wing embedded in a free stream at a chord based Reynolds number of 100, which is within the range of insect flight. This study utilizes the same LBFPM as investigated by Qi et al[16] and Qi and Liu [17] to examine how flexibility affect lift and drag forces and power efficiency as well as fluid structures at a given pitch rate. Further, with variation of pitch rates, their effects on lift and drag forces at different levels of flexibility can be systematically studied. Therefore, information about flight performance due to flexibility could be extracted and analyzed and the question "how do insets use their flexibility to improve lift and power efficiency" will be partially answered in the present work.

The next section will briefly introduce the simulation method and the canonical kinematics. The section 3 will present the results of lift and drag forces and power efficiency at different levels of flexibility and pitch rate. Simultaneously influence of flexibility on flow structures will be reported. The conclusions will be made in the last section.

2 Simulation method

In general, the algorithm of the LB method for simulating a fluid domain is extremely simple and consists of only two operations, collision and streaming. It has been demonstrated that the LBFPM is particularly suitable for simulations of flexible bodies in fluid flows. The LBFPM has been reported in details elsewhere by Qi [15] and Qi et al[16] and will not be repeated here. In this method, the body of the wing has been discretized into a chain of rigid beam segments. The segments are connected through ball and socket joints at the segment ends as shown in figure 1. Bending and twisting of the

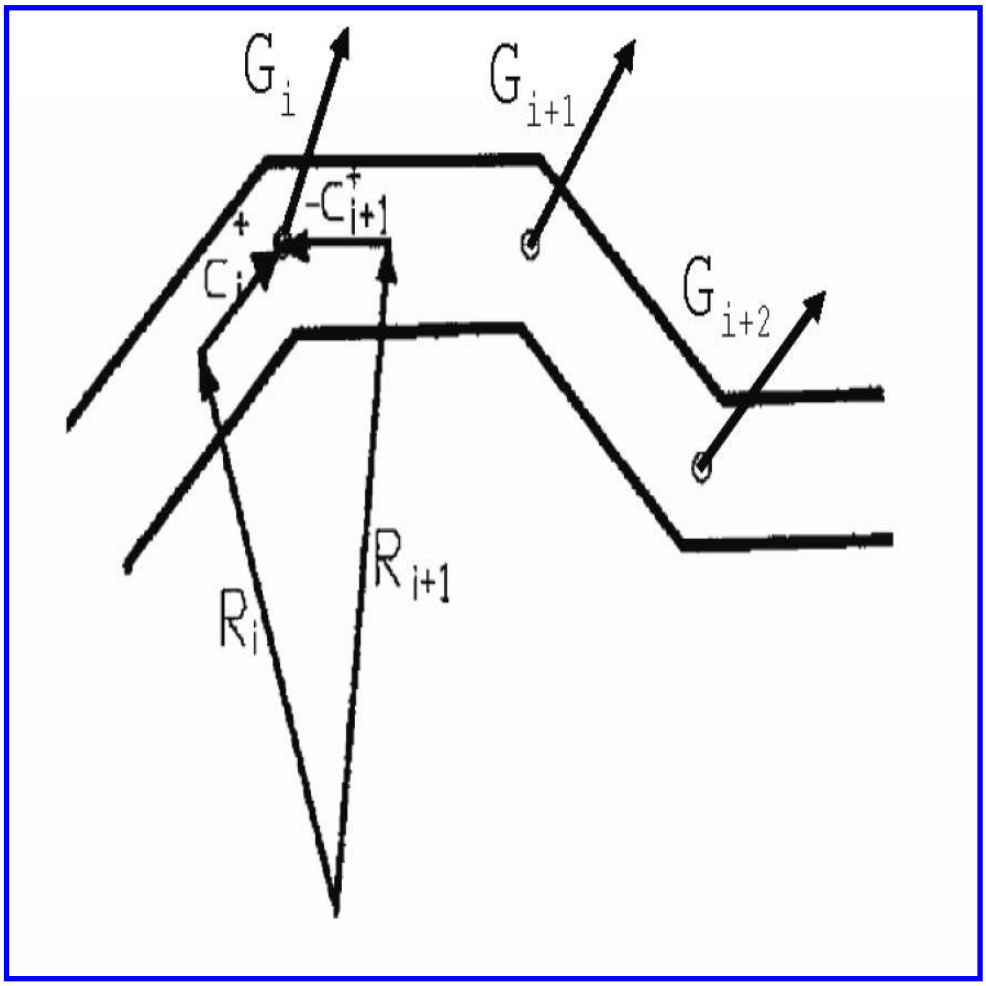

Figure 1: The beam segments are connected through ball and socket joints [circles].

wing are obtained through relative rotation between neighboring segments. Constraint forces have been introduced at each joint to ensure that the segments are connected to each other. The motion of fluid and its interactions with solid boundaries are handled by the lattice Boltzmann equation. The validation of the LBFPM was extensively provided by comparing its results with experimental and numerical results of Toomey and Eldredge[12]. It has been demonstrated that the LBFPM is faithful and replicates the correct physics of flow response to deformable either span-wise or chord-wise flexible wing. This method will be used here again.

2.1 Kinematics

A flexible wing is subjected a pitch-up and pitch-down motion in an incompressible fluid with a density of ρ_f and a kinematic viscosity of ν at a chord based Reynolds number of 100 in a free stream flow with a velocity of U_0.

The wing with a rectangular cross section could be described either in a space-coordinate system (X,Y,Z) or a body-fixed coordinates system. The body-fixed coordinates (X',Y',Z') can be transferred to the space coordinates (X,Y,Z) through the Euler angles ϕ, θ, and ψ [30] if rotation is imposed. Initially the body-fixed coordinate system (X',Y',Z') overlaps with the space coordinate system (X,Y,Z). The flexible wing is placed in the center of the simulation box such that the span s is along the Z'-direction; the chord c along the X'-direction; the wing thickness of T along the Y'-direction.

The wing is uniformly discretized along the span as N segments. At this stage, whole the wing is rotated by $\theta = 90^0$ around the X-axis. As a result, the wing span is oriented along the Y-direction in the space coordinate system as shown in figure 2.

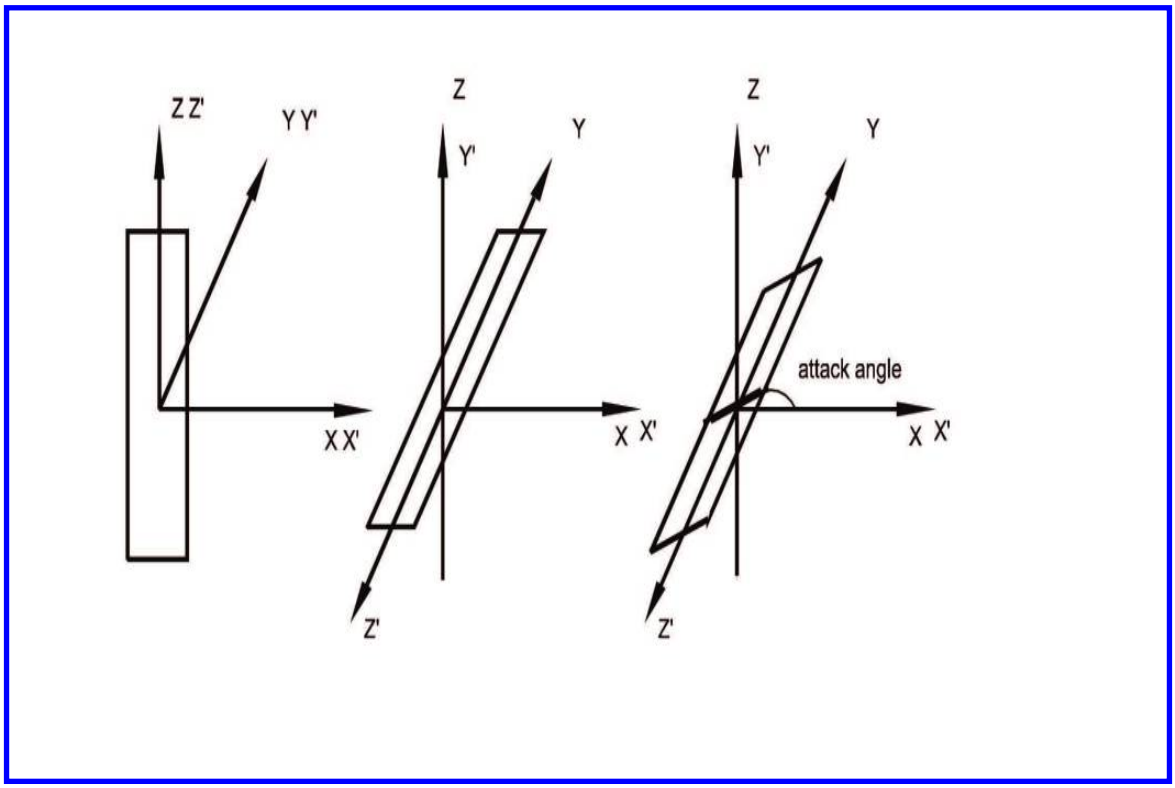

Figure 2: The root segment is alway fixed in the body-coordinate system (X', Y', Z'). Initially the wing is along the Z'-axis. After rotating 90^0 around X axis, the wing span is along Y axis. The wing is plunging in X or horizontal direction and rotating around Z' or -Y axis.

Thus, the angle ψ of the root segment spinning around its Z' or -Y axis is the pitch angle or the angle of attack. Following Eldredge work[31], this pitch angle is pre-described and given by

$$\psi(t) = \psi_0 \frac{G(t)}{maxG} \tag{1}$$

where ψ_0 is the maximum of the pitch angle and G describes a complete pitch-up and pitch-down maneuver,

$$G(t) = ln[\frac{cosh(aU_0(t-t_1)/c)cosh(aU_0(t-t_4)/c)}{cosh(aU_0(t-t_2)/c)cosh(aU_0(t-t_3)/c)]}. \tag{2}$$

The parameter a control the speed of the pitch transition between kinematic intervals, with larger values producing sharper transitions. A moderate value of 11 throughout the present study is used. The times t_1, t_2, t_3, t_4 represent transition instants during the maneuver: t_1 is the start of the pitch-up, $t_2 = t_1 + \psi_0/\dot{\psi}_0$ is the end of the pitch-up, $t_3 = t_2 + \Delta T$ is the start of the ensuing pitch-down; and $t_4 = t_3 + \psi_0/\dot{\psi}_0$ the end of the pitch-down where $\dot{\psi}_0$ is the pitch rate; c is the chord length. The reduced frequency κ is defined by $\kappa = \dot{\psi}_0 c/(2U_0)$.

Previously, a similar kinematic function of the pitch-ramp-return was employed to drive a flexible 2D beam flapping by Toomey and Eldredge [12], and their experimental and numerical results were used to validate the LBFPM (see figure of 9 reference[16]). Now, the exact same case as figure 5 of Eldredge and Wang's article [31] is run by using the lattice Boltzmann method and the results of lift and drag coefficients are compared and presented in figure3. A good agreement between the two results further validates the lattice Boltzmann method with the pitch-ramp-return kinematic function.

In the present work, pitch starts at $t_1 = c/U_0$, the parameters are fixed at $\psi_0 = 45^0$, $\theta = 90^0$, $\phi = 0^0$, $s/c = 2.5$. The reduced frequency is varied at $\kappa = 0.2, 0.7, 1.0$ and 1.25. Two holding time are used, one is short $\Delta T = 0.05c/U_0$, other is longer $\Delta T = c/U_0$. The wing is always flapping around the central axis of the chord for all simulations. The wing thickness is fixed at $T = 0.075c$; the number of segments is $N = 9$; the simulation box size is $(N_x, N_y, N_z) = (240, 200, 240)$ and the wing with $s = 100$ and $c = 40$ is used. These selected simulation resolutions for the box and wing sizes and the number of the segments were tested in the previous publication[16] and will be used here again.

In the present work, the chord based Reynolds number is defined by

$$Re = \frac{U_0 c}{\nu} \tag{3}$$

and the rotational Reynolds number is defined by

$$Re_r = \frac{\dot{\psi} c^2}{\nu}. \tag{4}$$

The lift coefficient is defined by

$$C_l = \frac{F_z}{0.5\rho_f U_0^2 sc} \tag{5}$$

where F_z is the vertical component of the total hydrodynamic force on the wing. The drag coefficient is defined by

$$C_d = \frac{-F_x}{0.5\rho_f U_0^2 sc} \tag{6}$$

where F_x is the horizontal component of the total hydrodynamic force on the wing.

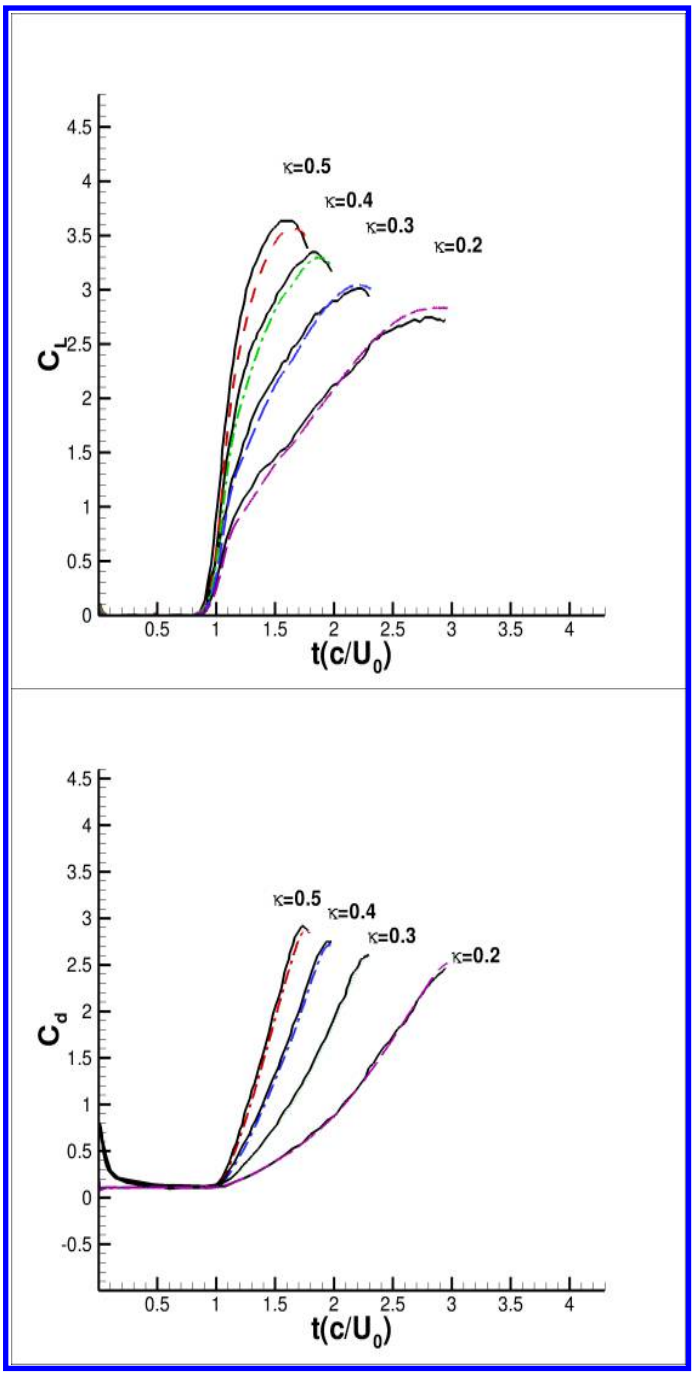

Figure 3: The lift (top) and drag coefficients (bottom) as a function of time during pitch-up motion at $\kappa = 0.5$, 0.4, 0.3, 0.2 are compared with those (solid lines) of Eldredge and Wang[31] at $Re = 1000$. The non-solid lines present the lattice Boltzmann method results. Two grids of 2000×2000 and 1600×1600 are used and the results are little different.

There are two parameters that control the wing flexibility: the bending flexural rigidity EI_w and the twisting or torsional rigidity GI_p. They can be normalized by

$$EI = \frac{EI_w}{0.5\nu\rho_f U_0 s^3} \tag{7}$$

and

$$GI = \frac{GI_p}{0.5\nu\rho_f U_0 s^3}. \tag{8}$$

GI is fixed at a large value of $13,700$ to ensure a neglected torsion deformation while EI is varied at different levels. The ratio of the wing density to the fluid density is fixed at $\rho_s/\rho_f = 16.27$. the density of solid

3 Results

3.1 Flexibility on lift and drag forces

Flexion of the wing in the span direction was observed decades ago [32]. The flexion often occurs at the end or beginning of stroke. Several functions of the flexion were hypothetically suggested. Although recent numerical simulations have shown that the combination of bending with rotation may benefit lift, controversy exists. For example, the experiments (see page 1960 of [33]) did not observed an increase in lift due to spanwise flexibility.

To understand rotational or pitch effect on lift and drag, at a given reduced frequency, the lift and drag coefficients are computed at different levels of the bending flexural rigidity while keeping other conditions same. The results of lift and drag coefficients as a function of time within a pitch-up and pitch-down interval at three different levels of bending flexural rigidity are shown in figure 4 for the cases of $\kappa = 1.25$. The kinematics of pitching angle is also shown in the figure. It can be seen that all the peaks of the force curves at the three levels of the rigidity have a phase lead to the pitch angle function as expected. The phase lead is due to the acceleration peak (added mass) of the rotation (or pitch) that appears in the very earlier stage of the time in the pitch-ramp-return function. This has been clearly explained by Ol et al (see figure 2 of reference[20]).

As the value of the bending flexural rigidity decreases from an infinite large (corresponding to a rigid wing) to the value of $EI = 223.42$, the right shoulder of the peak of the lift coefficient curve shifts to the right side and becomes more wide as compared with the rigid wing (see figure 4). The average lift coefficient over the time interval of the entire pitch-up and pitch-down motion is $C_l = 1.753$ for the flexible wing of $EI = 223.42$ and $C_l = 1.412$ for the rigid wing. In other words, with pitch or rotation the flexibility results in a 24% increase in lift as compared with the rigid wing, although the maximum value of the peak is smaller for the flexible wing than for the rigid wing. It is clear that the widened right shoulder of the lift curve has more positive values for the flexible wing with the optimized flexural rigidity of $EI = 223.42$ than for the rigid wing. However, when the wing becomes excessively flexible, for example, the rigidity becomes $EI = 11.17$, its lift coefficient reduces to $C_l = 1.01$. In this case, the lift curve becomes narrower and shorter. The drag coefficient has a similar behavior. But, the maximum of the drag $C_d = 1.48$ occurs at the slightly larger flexibility of $EI = 288.49$.

To further distinguish the different effects of the flexibility on the pitch-up motion and on the pitch-down motion, the lift and drag coefficients are computed and averaged over the pitch-up time period between t_1 and t_2 and over the pitch-down time period between t_2 and t_4, respectively, so that the force coefficient is divided into two portions: one called a pitch-up lift coefficient and other called a pitch-down lift coefficient. The

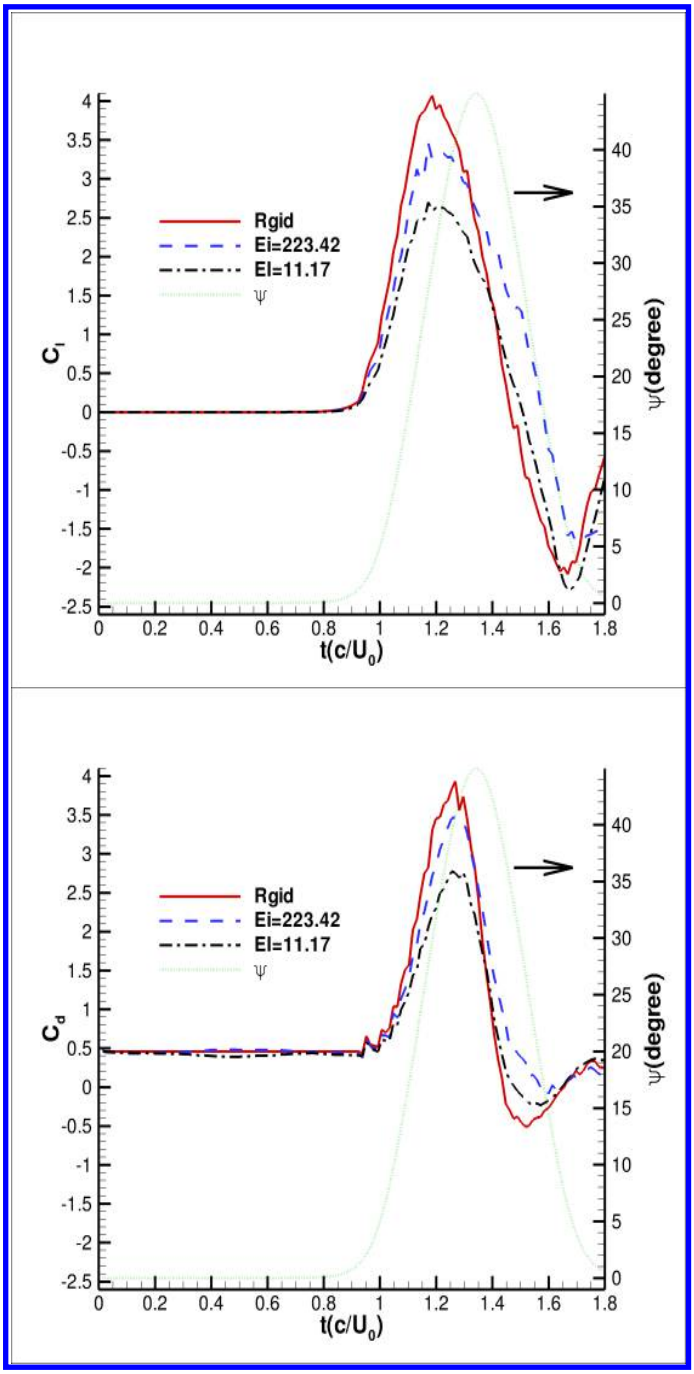

Figure 4: The lift coefficient (top) and drag coefficient (bottom) as a function of time during the time interval between t_1 and t_4 at three different levels of the wing rigidity (rigid ; $EI = 223.42$; $EI = 11.17$) at $\kappa = 1.25$. The pitch angle as a function of time is also shown on the right vertical axis where the arrow points to the angle scale. The pitch-up starts at $t_1 = U_0/c$ and the pitch-down ends at $t_4 = 1.6785U_0/c$.

results of the lift coefficient C_l along with the pitch-up lift coefficients, C_l^u, and the pitch-down lift coefficient, C_l^d, as a function of EI are shown in figure 5 for the case of $\kappa = 1.25$. The figure shows that C_l increases first as the values of EI decreases, then decreases. There is a maximum at $EI = 223.42$, indicating that the optimization of flexibility is necessary. It is remarkable that the pitch-up lift continuously decreases as the flexural rigidity decreases, suggesting that the flexibility does not improve lift during pitch-up rotation. In fact, the flexibility has a negative effect on lift through pitch-up rotation. On contrary, the pitch-down coefficient increases first as the flexural rigidity decreases, then falls down. Its maximum peak appears clearly. It is surprised that the pitch-down lift coefficient is $C_l^d = 0.974$ for the flexible wing of $EI == 223.42$ and significantly larger than $C_l^d = -0.125$ for the rigid wing, demonstrating that the flexibility is able to convert a negative lift coefficient for the rigid wing to a large positive value for flexible wing by using the pitch-down motion. It is demonstrated that the increase in lift due to flexibility is dominated by the pitch-down rotation, not by the pitch-up. In short, the enhancement in lift due to flexibility occurs only during the pitch-down motion.

The force coefficient results are also obtained and displayed in figure6 for the case of $\kappa = 1.0$ and in figure7 for the case of $\kappa = 0.7$. All the lift forces have maximum and the similar behavior as the case with the high rate of $\kappa = 1.25$. However, a comparison among figures 5, 6 and 7 shows that the rotation rate has an important impact on the forces. It looks that a larger pitch rate results in a larger lift force and that the lift increases due to flexibility as the pitch rate increases. The lift force increases a 24% for the case of $\kappa = 1.25$, a 20% for the case of $\kappa = 1.0$, and a 13% for the case of $\kappa = 0.7$, as compared with their corresponding rigid wings.

When the pitch rate is low, say $\kappa = 0.2$, the lift force remains at almost the same level as the flexural rigidity reduces, then drops to a very low level when the flexural rigidity becomes excessively small, illustrating that when the pitch rate is low, the flexibility may not significantly improve the lift, as shown in figure 8. In other words, a large rotation rate is required for flexibility to significantly improve lift.

3.2 Deformation and vortices

Dynamic interaction between the deformation of a flexible wing and fluid flows may alter the fluid structures and lift and drag forces. The deformation may be measured by a deflection ratio of the distance between the undeformed and deformed wing tips to a half of span length. This deflection ratio as a function of time is plotted in figure 9 and the pitch angles are shown in the same figure. The maximum deflection is only about 4.5% for the optimized flexible wing of $EI = 223.42$. The deformation is much smaller as compared with the hovering flapping wing case[16] where the deflection ratio could be as large as 30%. Also, the time of maximum deformation does not coincide with that of the maximum of the pitching angle. The maximum deformation shifts to a later time and occurs after beginning of pitch down.

The vorticity is computed for the flexible and rigid wings. The iso-surfaces of vorticity magnitude are plotted at three different time instances $t = 1.45c/U_0$, $1.57c/U_0$ and $1.65c/U_0$ during pitch-down period in figure10 for the value of the iso-surface of $p = 0.4$, in figure11 for $p = 0.3$ and in figure11 for $p = 0.2$. In these figures, the wings in the same row are at the same instance; the left for the flexible wing is compared with the right for the rigid wing. It is obviously seen that the flexible wing has not only larger LEV but also larger TEV. In particular, the TEV is well developed for the flexible wing along the wing tip top surface, implying that the small span-wise flexibility induces considerably large TEV. The areas and volumes covered by LEV and TEV are larger for the flexible wing than the rigid wing. The difference increases as time increases, suggesting that the vortex separation is smaller for the flexible wing than for the rigid

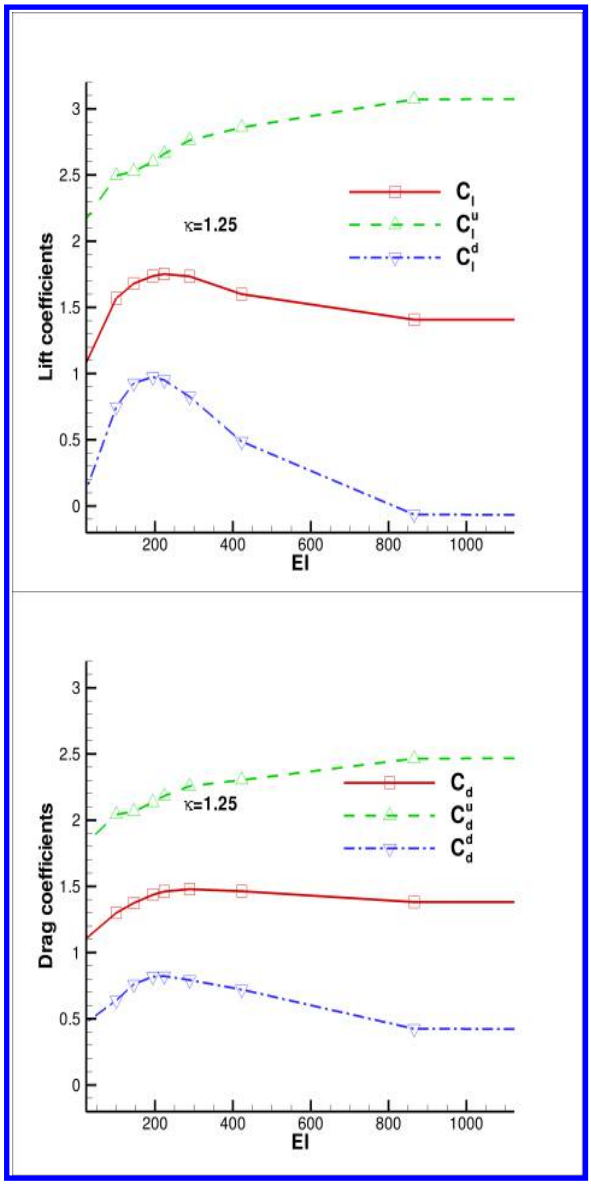

Figure 5: a) The lift coefficient C_l along with the pitch-up lift coefficient C_l^u and the pitch-down lift coefficient C_l^d b) their corresponding drag coefficient as a function of the flexural rigidity for the case of $\kappa = 1.25$.

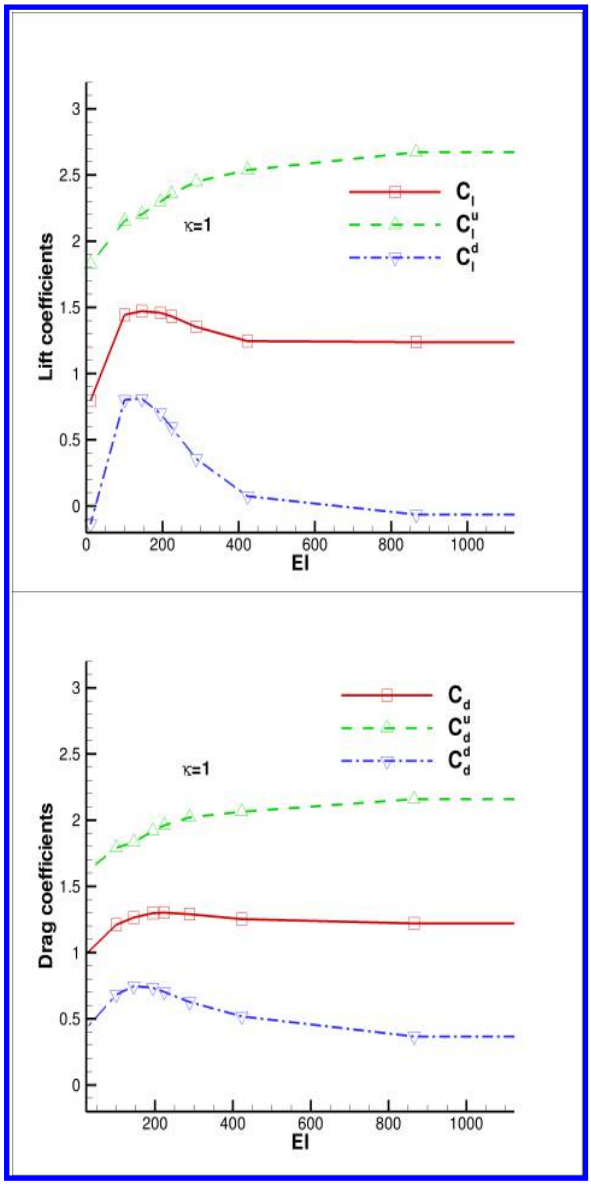

Figure 6: a) The lift coefficient C_l along with the pitch-up lift coefficient C_l^u and the pitch-down lift coefficient C_l^d b) their corresponding drag coefficient as a function of the flexural rigidity for the case of $\kappa = 1.0$.

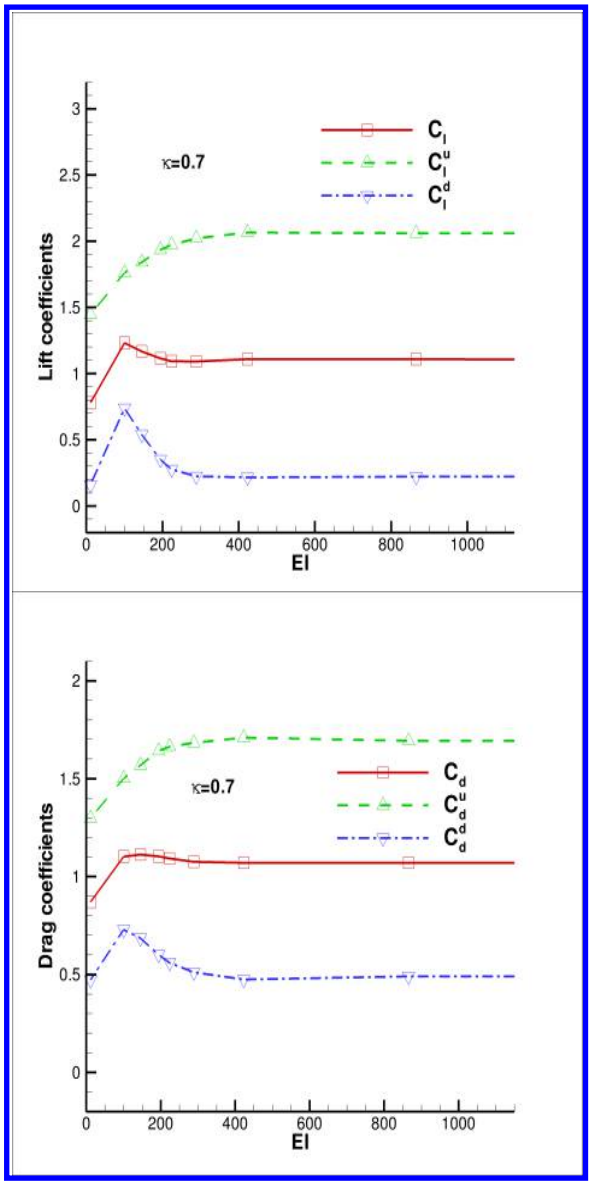

Figure 7: a) The lift coefficient C_l along with the pitch-up lift coefficient, C_l^u, and the pitch-down lift coefficient, C_l^d, b) their corresponding drag coefficient as a function of the flexural rigidity for the case of $\kappa = 0.7$.

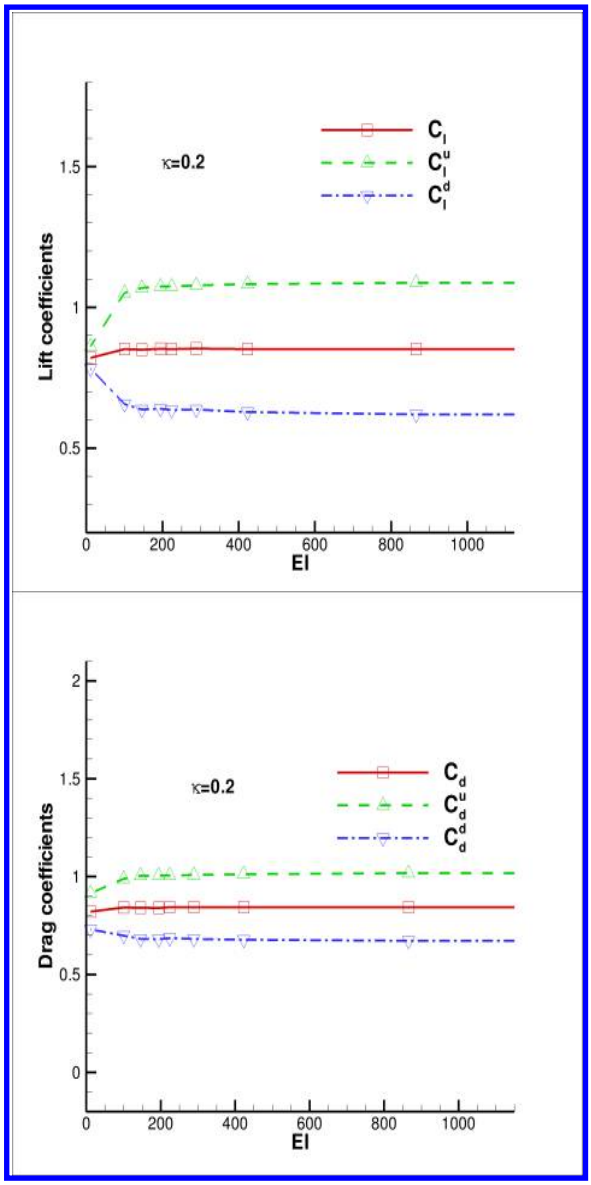

Figure 8: a) The lift coefficient C_l along with the pitch-up lift coefficient, C_l^u, and the pitch-down lift coefficient, C_l^d, b) their corresponding drag coefficient as a function of the flexural rigidity for the case of $\kappa = 0.2$.

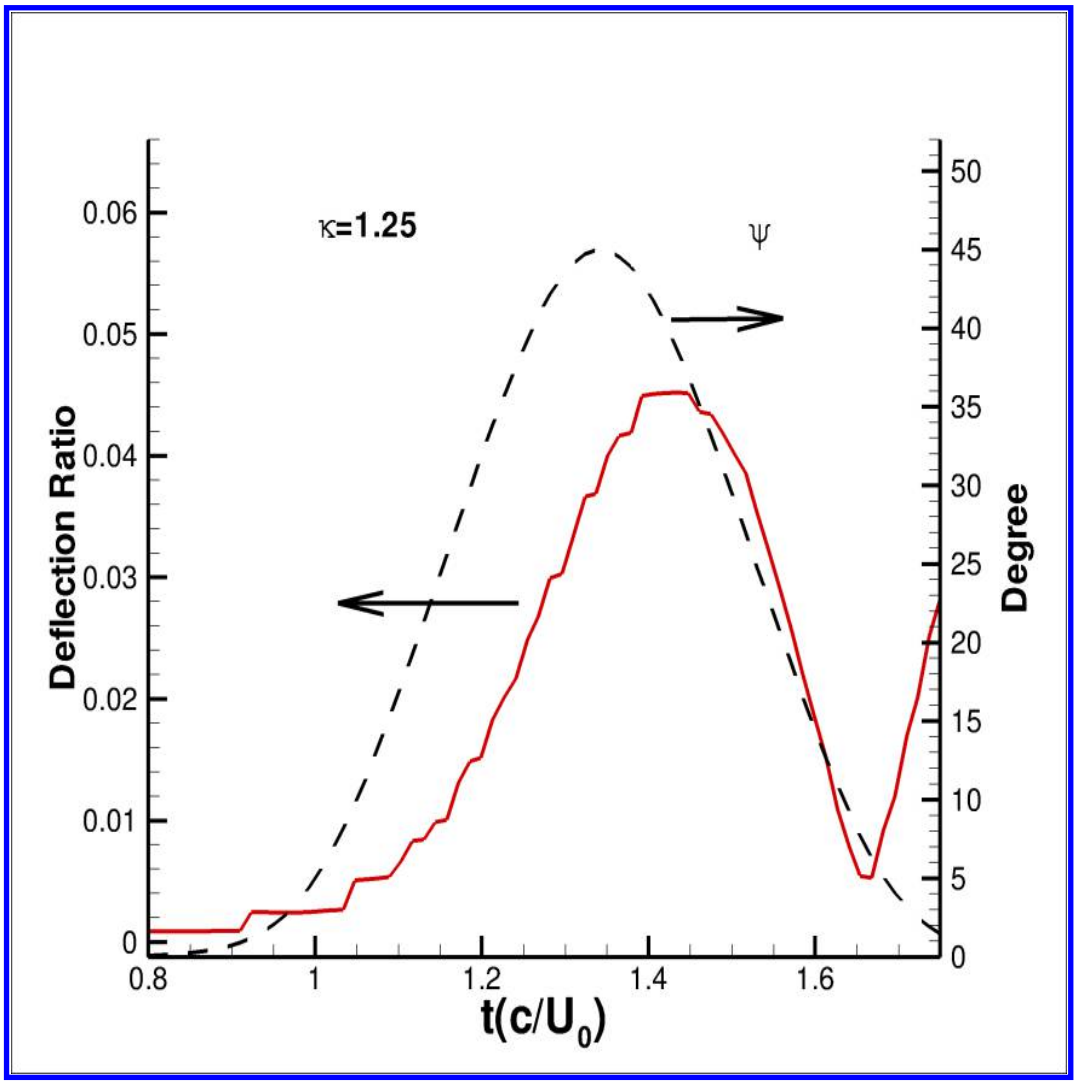

Figure 9: The deflection ratio along with pitch angles is plotted as a function of time for the flexible wing of $EI = 223.42$. The solid line is for the deflection ratio and the broken line is for the pitch angle.

wing.

In order to further understand why the pitch-down motion enhance the lift, a simulation of the wing with $EI = 223.42$ and $\kappa = 1.25$ is conducted at the same condition except using a longer hold time $\Delta T = c/U_0$ so that the pitch-up motion is stopped at $t = t_2 = 1.314c/U_0$, hold for a longer time period of c/U_0, then becomes pitch-down. The results of lift force for the flexible wing are plotted and compared with the rigid wing in figure 13. It is shown that after the wing pitch-up or rotation is stopped at $t = t_2 = 1.314c/U_0$ the lift force still remains positive and is larger for the flexible wing than the rigid wing until $t = t_c = 1.72c/U_0$. The average lift coefficient between t_2 and t_c is 1.16 for the rigid wing and 1.36 for the flexible wing, 17% larger for the later one, illustrating that the lift force is diminishing much slower for the flexible wing at the earlier stage of the pitch-up rotation is stopped. Although the lift becomes smaller between $t = t_c = 1.72c/U_0$ and $t = t_d = 2.15c/U_0$ (see figure 13 for t_c and t_d) for the flexible wing, the average lift coefficient over all the time period is 1.49 for the rigid wing and 1.57 for the flexible wing.

The differences of the iso-surfaces of vorticity between the optimized flexible wing and rigid wing are compared in figures 14 and 15. Two instances are shown in these figures: one is $t = t_a = 1.61c/U_0$ (top row) within the holding-time period and other is $t = t_b = 2.42c/U_0$ (bottom row) during the pitch-down time period. The left for the optimized flexible wing is compared with the right for the rigid wing at the same instance in the same row. Clearly, the flexible wing has much larger vortices located on the tip edges of the wing surface than the rigid wing at $t = t_a$ within the holding time. The vortices covers not only the leading edge surface but also the wing tip edge surfaces. At this time instance although the wing pitch is stopped, the vortices on the wing surface are still larger for the flexible wing, evidencing that the flexibility enhances the vortices. At t_b during the pitch-down motion, the vorticity are still larger for the flexible wing than for the rigid wing. Reasonably, the surface areas covered by the vortices at time $t = t_b$ are reduced as compared with those at the previous time instance $t = t_a$ due to vortex separation. However, such the reduction is smaller for the flexible wing due to flexibility retarding the vortex separation.

Most likely, flexibility can dynamically and passively adjust the trailing edge positions along span direction. According to Kutta-Joukowski theorem, the flows will separate in the trailing edge due to Kutta condition and form trailing edge vortices which are shedding to wake area and benefit lift[34]. In other words, the trailing edge position change in a flexible wing induces a larger LEV and TEV and a larger trailing edge vortex shedding and enhances lift.

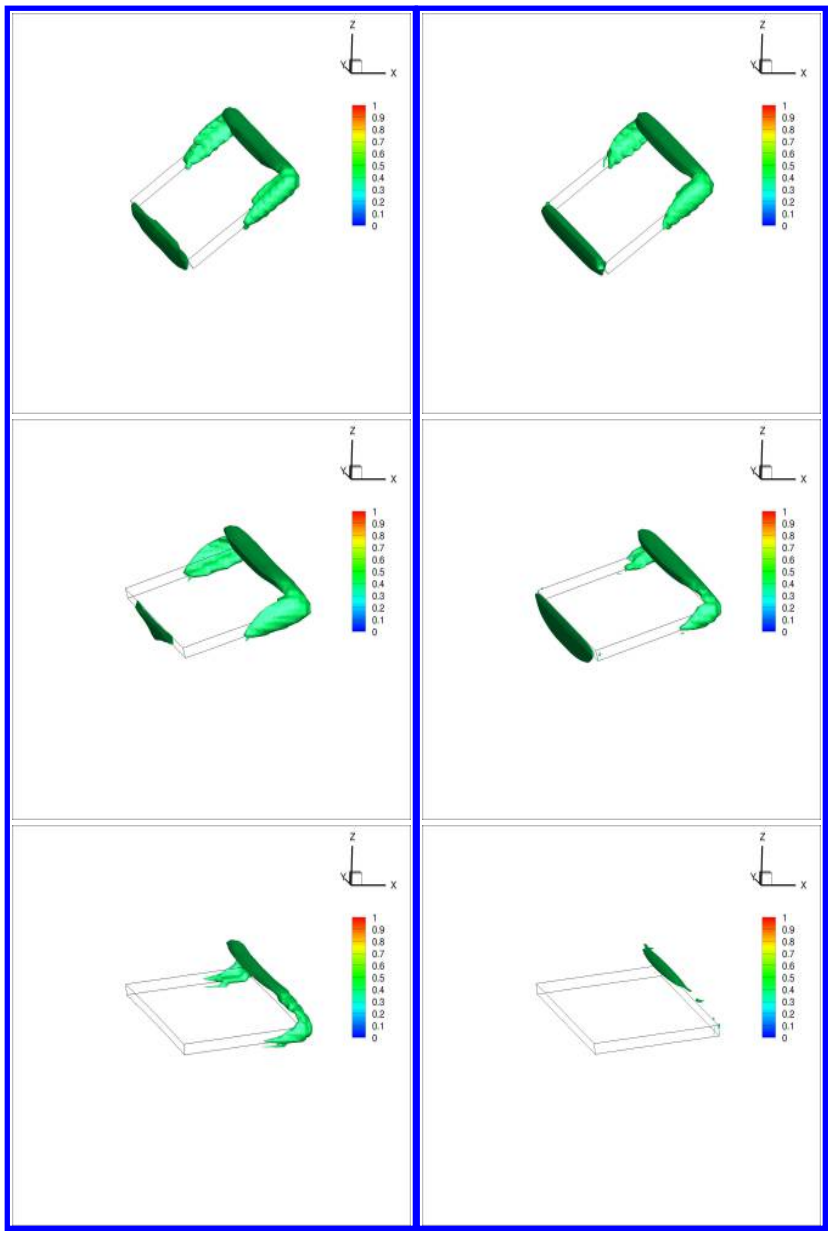

Figure 10: The iso-surfaces of the vorticity (normalized by the maximum value) for the flexible case (the left colum) of $EI = 223.42$ are compared with those for a rigid wing (right colum) at different time instances $t = 1.45c/U_0$ (top row), $t = 1.57c/U_0$ (middle row) and $t = 1.65c/U_0$(bottom row) during the pitch-down time period. The iso-value of the vorticity is 0.4.

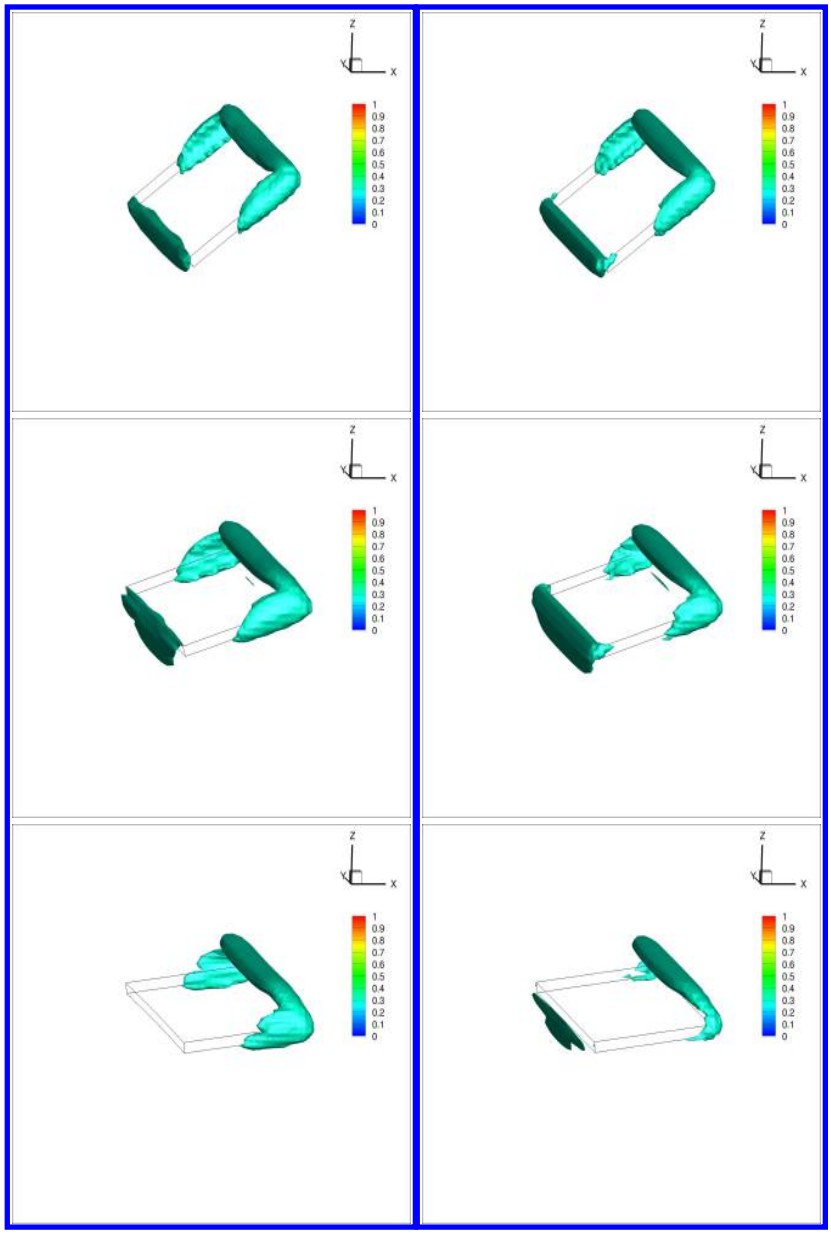

Figure 11: The same as figure 10 except that the value of the iso-surface is 0.3

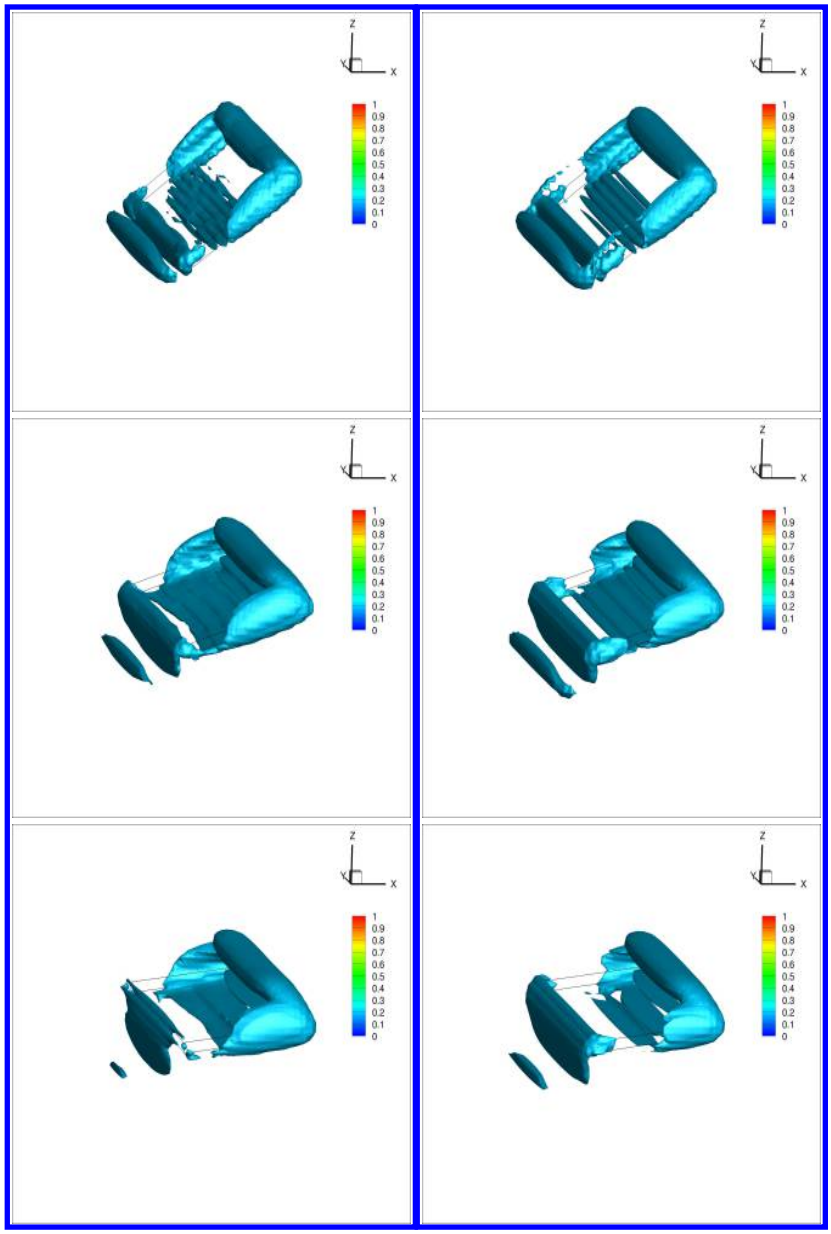

Figure 12: The same as figure 10 except that the value of the iso-surface is 0.2

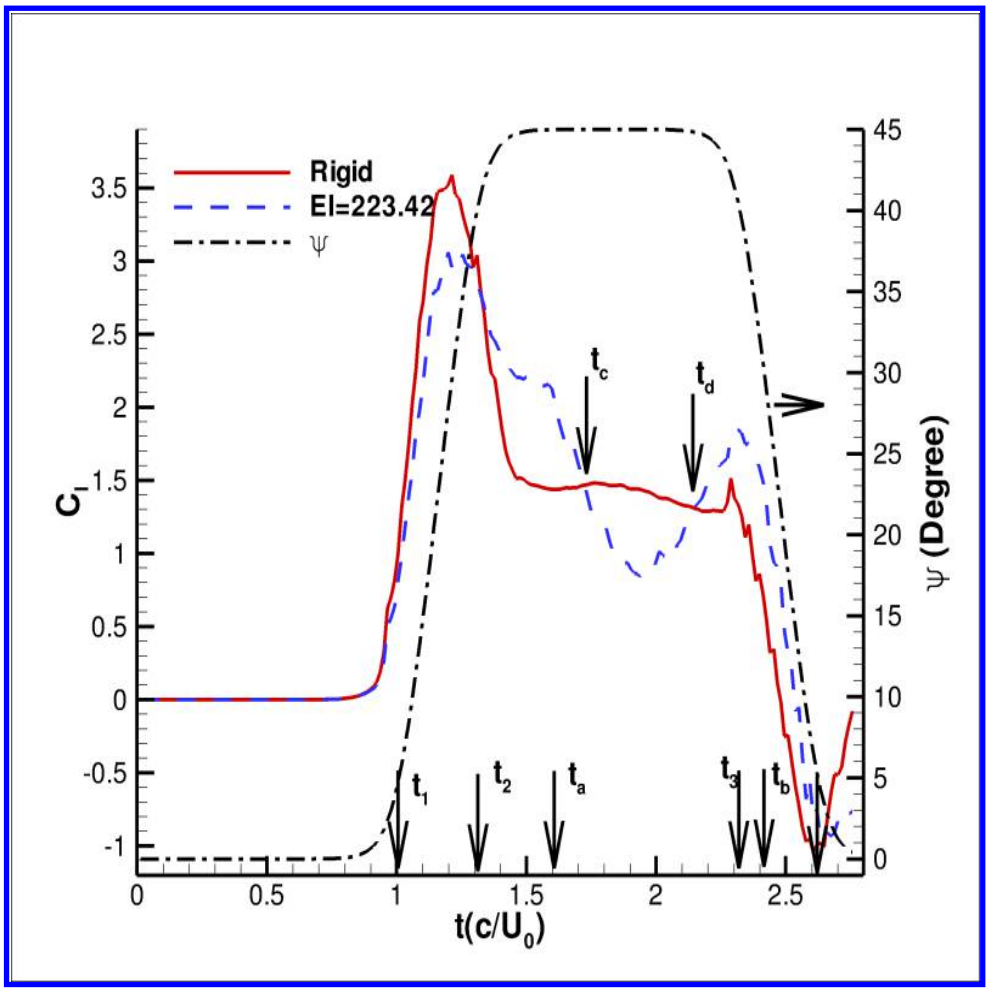

Figure 13: The lift coefficient of the flexible wing as a function of time is compared with the rigid wing where the hold time is $\Delta T = c/U_0$.

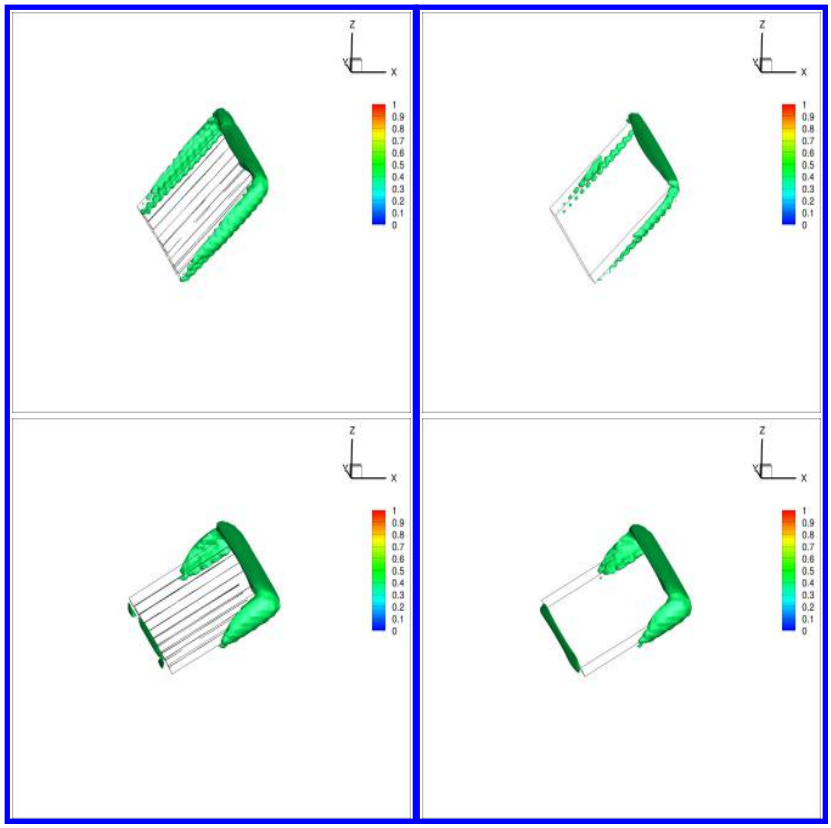

Figure 14: The iso-surfaces of the vorticity (normalized by the maximum value) for the flexible case (the left colum) of $EI = 223.42$ are compared with those for a rigid wing (right colum) at $t = t_a = 1.61c/U_0$ (top colum) and $t = t_b = 2.42c/U_0$ (top row). t_a and t_b are shown in figure13. The value of the iso-surface is 0.4.

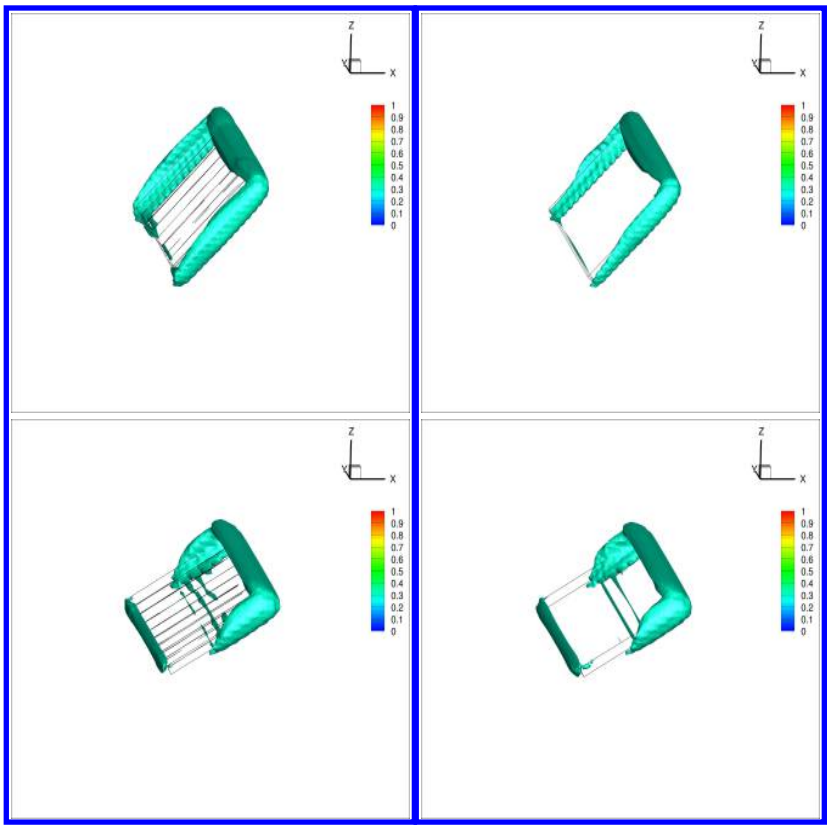

Figure 15: The same as figure 14 except that‘ the value of the iso-surface is 0.3.

4 Conclusions

The direct simulations of the pitch-up and pitch-down of flexible and rigid wings in a free stream are conducted at the Reynolds number of $Re = 100$ by using the LBFPM. The effect of bending flexibility in span-wise direction on unsteady aerodynamics are investigated. The following conclusions can be made from the cases with the selected kinematic parameters.

1. It is found that when the reduced frequency is large, the lift and drag forces increase nonlinearly upto a maximum as the flexibility increases, then falls down as the flexibility becomes excessively large. The maximum value in both lift and drag forces are significantly larger for a flexible wing than for a rigid wing. However, when the reduced frequency is small, no obvious lift maximum is observed. It seems that flexibility can be used to enhance the lift force at a high reduced frequency.

2. It is surprised that flexibility improves lift only during pitch-down motion while the flexibility has a negative impact on lift during pitch-up motion, indicating that the pitch-down motion dominates the lift improvement due to flexibility.

3. In a maneuver case, a small and adequate span deformation may change trailing edge position along span direction and enhance circulation due to Kutta condition. The larger LEV and TEV and the larger trailing vortices shedding benefit lift.

A valuable discussion with Dr. Eldredge is appreciated.

References

[1] M.J.C. Smith. Effect of spanwise flexibility on the aerodynamics of moth wings: Toward the development of flapping-wing technology. *AIAA Journal*, 34:1348–1355, 1996.

[2] S. Heathcote and I. Gursul. Flexible flapping airfoil propulsion at low reynolds numbers. *AIAA J*, 45:1066, 2007.

[3] S. Heathcote, Z. Wang, and I. Gursul. Effect of spanwise flexibility on flapping wing propulsion. *Journal of Fluids and Structures*, 24:183–199, 2008.

[4] S. Heathcote, D. Martin, and I. Gursul. Flexible flapping airfoil propulsion at zero free stream. *AIAA Journal.*, 42:2196–2204, 2004.

[5] K.D. Frampton, M. Goldfarb, D. Monopoli, and D Cveticanin. *Passive Aeroelastic Tailoring for Optimal Flapping Wings, Fixed and Flapping Wing Aerodynamics for Micro Air Vehicle Applications, Edit by T. J. Muller*, volume 195. Progress in Astronautics and Aeronautics, AIAA, New York, 2001.

[6] S. Chimakurthi, J. Tang, R. Palacios, C. Cesnik, and W. Shyy. Computational aeroelastic framework for analyzing flapping wing micro air vehicles. *AIAA Journal*, 47:1865–1878, 2009.

[7] W. Shyy, Y. Lianand J. Tang, D. Viieru, and H. Liu. *Aerodynamics of Low Reynolds Number Flyers*. Cambridge University Press, New York, 2008.

[8] W. Shyy, Y. Lian, J. Tang, H. Liu, P. Trizila, B. Stanford, L.P. Bernal, C.E.S. Cesnik, P. Friedmann, and P. Ifju. Computational aerodynamics of low reynolds number plunging, pitching and flexible wings for mav applications. *Acta Mechanica Sinica*, 24:351–373, 2008.

[9] W. Shyy, H.Aono, S. K. Chimakurthii, P. Trizila, C. K. Kang, C.E.S.Cesnik, and H.Liu. Recent progress in flapping wing aerodynamics and aeroelasticity. *Progress in Aerospace Sciences*, 2010.

[10] J. Tang, S. Chimakurth, R. Palacios, C.E.S. Cesnik, and W. Shyy. Computational fluid-structure interaction of a deformable flapping wing for micro vehicle applications. *46 AIAA Aerospace Science Meeting and Exhibit, 7-10 January, Reno, Nevada*, page 123, 2007.

[11] W. Shyy, P. Trizila, C. Kang, and H Aona. Can tip vortices enhance lift of a flapping wing. *AIAA J*, 47:289, 2009.

[12] J. Toomey and J. D. Eldredge. Numerical and experimental study of the fluid dynamics of a flapping wing with low order flexibility. *Phys of Fluid*, 30:073603, 2008.

[13] J. D. Eldredge, T. Toomey, and A. Medina. On the roles of chord-wise flexibility in a flapping wing with hovering kinematics. *J Fluid Mech.*, 659:94–115, 2010.

[14] M. Vanella, T. Fitzgerald, S. Predikman, E. Balaras, and B. Balachandran. Influence of flexibility on the aerodynamic performance of a hovering wing. *J Exp. Biol.*, 212:95–105, 2009.

[15] D. Qi. Direct simulations of flexible cylindrical fiber suspensions in finite reynolds number flows. *J. Chem. Phys.*, 125:114901–10, 2006.

[16] Dewei Qi, Yingming Liu, Wei Shyy, and Hikaru Aono. Simulations of dynamics of plunge and pitch of a 3d flexible wing in a low reynolds number flow. *Physics of Fluids*, 22:091901, 2010.

[17] D. Qi and Y. Liu. Simulations of dynamics of plunge and pitch of a 3d chord-wise flexible wing in a low reynolds number flow. In *49th AIAA Aerospace Sciences Meeting Including the New Horizons Forum and Aerospace Exposition*, page 221, Orlando, Fl, 4-7 January 2011. AIAA.

[18] M.H. Dickinson., F.O. Lehmann, and S. Sane. Wing rotation and the aerodynamic basis of insect flight. *Science*, 284:1954–1960, 1999.

[19] C.P. Ellington, C. Berg Van de, A.P. Willmott, and A.L.R. Thomas. Leading-Edge Vortices in Insect Flight. *Nature*, 384:626–630, 1996.

[20] M. V. OL, A. Altman, J. D. Eldredge, D. J. Garmann, and Y. Lian. Resume of the aiaa fdtc low reynolds number discussion group's canonical cases. In *48th AIAA Aerospace Sciences Meeting Including the New Horizons Forum and Aerospace Exposition*, page 1085, Orlando, Fl, January 2010. AIAA.

[21] J. Soria and K. Kilany. Multi-component, multi-dimensional piv measurements of low reynolds number flow around a flat plate undergoing pitch-ramp motion. In *the 39th AIAA Fluid Dynamics Conference*, page 3692, San Antonio, Texas, June 2009. AIAA.

[22] M. Ol. The high-frequency, high-amplitude pitch problem: Airfoils, plates and wings. In *the 39th AIAA Fluid Dynamics Conference*, page 3686, San Antonio, Texas, 2009. AIAA.

[23] D. Williams, S. Buntain, V. Quach, and W. Kerstens. Flow field structures behind a 3d wing in an oscillating free stream. In *the 39th AIAA Fluid Dynamics Conference*, page 3690, San Antonio, Texas, 2009. AIAA.

[24] Y. Lian. Parametric study of a pitching flat plate at low reynolds numbers. In *the 39th AIAA Fluid Dynamics Conference*, page 3688, San Antonio, Texas, 2009. AIAA.

[25] D. Garmann and M. Visbal. High fidelity simulations of transitional flow over pitching airfoils. In *the 39th AIAA Fluid Dynamics Conference*, page 3693, San Antonio, Texas, 2009. AIAA.

[26] J.D. Eldredge., C. Wang, and M. Ol. A computational study of a canonical pitch-up, pitch-down wing maneuver. In *the 39th AIAA Fluid Dynamics Conference*, page 3687, San Antonio, Texas, 2009. AIAA.

[27] X. Zhange, S.Z. Ni, S.Z. Wang, and G.W.He. Effects of geometric shape on the hydrodynamics of a self-propelled flapping foil. *Phys. Fluids*, 21:103302, 2009.

[28] Y. Lian and M.V. Ol. Experiments and computation on a low aspect ratio pitching flat plate. In *48th AIAA Aerospace Sciences Meeting Including the New Horizons Forum and Aerospace Exposition*, page 0385, Orlando, Fl, January 2010. AIAA.

[29] M. Ol, J.D. Eldredge, and C. Wang. High-amplitude pitch of a flat plate: an abstraction of perching and flapping. *Intl. J. MAVs*, 1:203, 2009.

[30] H. Goldstein. *Classical Mechanics*. Addison-Wesley Publishing Company, Cambridge, MA, 1980.

[31] J.D. ELdredge and C. Wang. High-fidelity simulations and low-order modeling of a rapidly pitching plate. In *40th Fluid Dynamics Conference and Exhibit, AIAA*, Chicago, IL, June 2010. AIAA-4281.

[32] R.J. Wootton. Support and deformability. *J Zool. Lond*, 193:447–468, 1981.

[33] J.M. Birch and M.H. Dickinson. Spanwise flow and the attachment of the leading-edge vortex on insect wings. *Nature*, 412:729–733, 2001.

[34] Y. Yu, B. Tong, and H. Ma. An analytic approach to theoretical modeling of highly unsteady viscus flow excited by wing flapping in small insects. *ACTA Mech, Sinca*, 19:508–516, 2003.